# Modeling strain-path changes in aluminum and steel

Jisheng Qin [a,*], Bjørn Holmedal [a], Kai Zhang [a], Odd Sture Hopperstad [b,c]

[a] Department of Materials Science and Engineering, Norwegian University of Science and Technology (NTNU), Alfred Getz vei 2, NO-7491 Trondheim, Norway

[b] Department of Structural Engineering, NTNU, Richard Birkelands vei 1a, NO-7491 Trondheim, Norway

[c] Centre for Advanced Structural Analysis (CASA), NTNU, Richard Birkelands vei 1a, NO-7491 Trondheim, Norway

qin_jisheng@hotmail.com, bjorn.holmedal@ntnu.no, kai.zhang@ntnu.no, odd.hopperstad@ntnu.no

*Corresponding author: Jisheng Qin, Tel.: +47 98067407

## Abstract

The present paper evaluates two phenomenological plasticity models which account for the influence of strain-path change (SPC) on the stress-strain behavior. The HAH model (Barlat et al., 2014) is modified to capture SPC transients observed in aluminum, i.e., hardening stagnation after reverse SPCs and permanent softening after orthogonal SPCs. Predictions by the HAH model are compared to the MHH model (Mánik et al., 2015), which was originally developed for aluminum. The MHH model turned out to be directly applicable to an extra deep drawing quality (EDDQ) steel without any modifications. The MHH model predicts the stress-strain behavior after single SPCs slightly better than the HAH model for both aluminum and steel. It can also capture correctly R-value transients in aluminum after purely orthogonal SPCs. However, only the HAH model can capture transients after double SPCs qualitatively for low carbon steels. The applicability of these advanced continuum plasticity models to aluminum and steel and the differences in their mathematical formulation are discussed.

**Keywords**: Strain-path change; Cross-hardening; Bauschinger effect; Permanent softening; HAH model

## 1. Introduction

An important part of forming simulations is the constitutive model, which should be as simple and efficient as possible, but still accurate enough to describe the material behavior. Due to memory effects related to the prestraining history, SPCs may cause extra transients of hardening or softening, which have to be properly accounted for in the modeling.

SPCs, which can be continuous or abrupt, are defined in terms of changes of the direction of the plastic rate-of-deformation tensor $\mathbf{D}^p$ or the deviatoric stress tensor $\boldsymbol{\sigma}'$. For abrupt SPCs, Schmitt et al. (1994) proposed the measure

$$\cos\phi_D = \frac{\mathbf{D}_1^p : \mathbf{D}_2^p}{\left\|\mathbf{D}_1^p\right\|\left\|\mathbf{D}_2^p\right\|} \tag{1}$$

while Barlat et al. (2011) used instead

$$\cos\phi_{\sigma'} = \frac{\boldsymbol{\sigma}_1' : \boldsymbol{\sigma}_2'}{\left\|\boldsymbol{\sigma}_1'\right\|\left\|\boldsymbol{\sigma}_2'\right\|} \tag{2}$$

Here, subscripts 1 and 2 refer to the strain path before and after the SPC, respectively, and further $\|\mathbf{T}\| = \sqrt{T_{ij}T_{ij}}$ denotes the norm of the second order tensor $\mathbf{T}$.

Typically, SPCs lead to transients in the stress-strain curve, but after a certain strain the monotonic behavior resumes. Bauschinger effect (Bauschinger, 1881; Hasegawa et al., 1975) and hardening stagnation (Boers et al., 2010; He et al., 2014) may be observed after reverse SPCs, while orthogonal hardening or softening (Ha et al., 2013; Hasegawa et al., 1975; Manopulo et al., 2015; Peeters et al., 2000; Tarigopula et al., 2008) may happen after orthogonal SPCs. However, the transients may sometimes influence the subsequent part of the stress-strain curve. An example of this type of behavior is permanent softening (Li and Bate, 1991). After double SPCs, the transients depend mainly on the orientation between the previous and subsequent paths and less on the order in which they have been performed (Vieira and Fernandes, 1995). These anisotropic hardening behaviors can, in general, be described by a yield surface that changes shape and size during plastic deformation. A recent review can be found in Mánik et al. (2015).

Two groups of models for SPCs have been suggested in the literature. In the first group, transients are modeled by shifting, expanding or shrinking the shape-invariant yield surface in

response to the SPC, by including a fading memory of the strain history. An important model based on this approach was proposed by Teodosiu and Hu (1995). Holmedal et al. (2010) proposed a plasticity model which applied second-order tensors to keep track of the strain history. The model was further modified by Mánik et al. (2015). In contradiction to the Teodosiu-Hu model, the permanent softening occurring after reverse or orthogonal loading is captured in this model. This modified model will henceforth be denoted the MHH model.

The other group of models modifies the shape of the yield surface. Hence, these models will be referred to as distortional models, e.g. Levkovitch and Svendsen (2007). A method for distorting any "stable" homogeneous yield surface was proposed by Barlat et al. (2011) as an alternative to kinematic hardening, which is denoted a Homogeneous Anisotropic Hardening (HAH) model. Lee et al. (2012) used the HAH model to describe the springback during U-draw bend experiments. Later the model was further extended and enhanced to capture the orthogonal hardening/softening behavior after single and double SPCs (Barlat et al., 2014, 2013; Ha et al., 2013; Lee et al., 2015).

The earlier published HAH models cannot capture permanent softening after orthogonal SPCs, which occurs in some materials. Reverse hardening stagnation has been modeled for pure Bauschinger cases (Barlat et al., 2011) based on a dislocation-based work-hardening model (Rauch et al., 2007). However, in this paper, the HAH model is further developed to include both reverse and orthogonal SPC behavior and thus to describe the type of transients observed in aluminum. The modified HAH model is then compared with the MHH model using earlier published experimental data for aluminum and steel, i.e., the stress-strain curves subsequent to complex SPCs for commercially pure aluminum reported by Mánik et al. (2015) and similar results presented by Ha et al. (2013) for an extra deep drawing quality (EDDQ) steel.

The EDDQ steel has high R-values, which makes it possible to distinguish between the two Schmitt angles $\phi_D$ and $\phi_{\sigma'}$, defined by Equations (1) and (2), respectively. The SPC experiments by Ha et al. (2013) indicate that the EDDQ steel exhibits a strong cross-hardening effect during orthogonal loading. The commercially pure aluminum investigated by Mánik et al. (2015) exhibits a strong and complex Bauschinger effect and also a strong cross-hardening effect. The EDDQ steel has earlier been modeled by the "extended" (Barlat et al., 2013) and "enhanced" (Barlat et al., 2014; Lee et al., 2015) HAH models, while commercially pure aluminum has been

modeled by the MHH model. Hence, a thorough evaluation of the capability of the enhanced HAH model and the MHH model to describe SPCs in aluminum and steel is of interest.

The current work begins with a brief review of the mathematical formulations of the MHH model and our modified version of the HAH model in Section 2. The parameter identification for the two models and a detailed comparison of simulation results and experimental data are presented in Section 3. In Section 4, the capability, differences and limitations of the two models are discussed. Finally, Section 5 presents the conclusions of the study.

## 2. Constitutive models

### 2.1 The MHH model

The MHH model modifies the yield surface by isotropic-kinematic hardening during plastic loading and by rapid expansion/shrinkage when the model detects a SPC. The yield condition is written in the form

$$\begin{aligned} f(\mathbf{S}) &\equiv \varphi(\mathbf{S}) - \bar{\sigma}(\bar{\varepsilon}) = 0 \\ \mathbf{S} &= \boldsymbol{\sigma} - \mathbf{X} \\ \bar{\sigma} &= R + S_o + S_r \end{aligned} \tag{3}$$

where $\mathbf{S}$ is the overstress tensor, $\boldsymbol{\sigma}$ is the stress tensor, $\mathbf{X}$ is the back stress tensor, $\bar{\sigma}$ is the size of the elastic range and $\bar{\varepsilon}$ is the equivalent plastic strain. The isotropic hardening is described by $R$, whereas $S_o$ and $S_r$ represent the extra yield surface expansion and shrinkage after orthogonal and reverse SPCs, respectively. The equivalent stress $\varphi(\mathbf{S})$ with respect to the back stress can be based on any positive homogeneous yield function of order one. In this study, the high-exponent Hershey yield function (Hershey, 1954) is used for initially isotropic materials, while the Yld2000-2d yield function (Barlat et al., 2003) is adopted for materials with initial anisotropy.

The associated flow rule is adopted and the plastic rate-of-deformation tensor is defined by using $\varphi(\mathbf{S})$ as a potential function, viz.

$$\mathbf{D}^p = \dot{\lambda} \frac{\partial \varphi(\mathbf{S})}{\partial \mathbf{S}} \tag{4}$$

where $\dot{\lambda} \geq 0$ is the plastic multiplier. The equivalent plastic strain $\bar{\varepsilon}$ is taken as

$$\bar{\varepsilon} = \int_0^t \dot{\lambda} dt \tag{5}$$

The microstructure orientation tensor $\mathbf{P}$, denoted the "delayed pointer" tensor in Mánik et al. (2015), is designed to memorize a representative direction in the strain-rate space and used in the modeling of relevant stress contributions from the recent microstructure evolution history. Its magnitude and direction are associated to the amount and orientation of dislocation structures. For well-annealed alloys, the magnitude of $\mathbf{P}$ equals zero. During monotonic loading, $\mathbf{P}$ saturates at a magnitude equal to unity. Its evolution is given by

$$\dot{\mathbf{P}} = \mathbf{h}_P \dot{\lambda}, \quad \mathbf{h}_P = \frac{1}{\Delta\varepsilon_P}\left(\mathbf{N} - \mathbf{P}\right) \tag{6}$$

where $\mathbf{N} = \mathbf{D}^p / \|\mathbf{D}^p\|$ is the normalized plastic rate-of-deformation tensor and $\Delta\varepsilon_P$ controls the strain scale of the evolution process of $\mathbf{P}$. The SPC between the memorized strain direction $\mathbf{P}/\|\mathbf{P}\|$ and the current strain path $\mathbf{N}$ is mathematically defined by the Schmitt angle

$$\cos\phi_P = \frac{\mathbf{P}}{\|\mathbf{P}\|} : \mathbf{N} \tag{7}$$

The extra strength due to the orthogonal and pseudo-orthogonal SPC is described by a scalar $S_o$ with evolution equation

$$\dot{S}_o = \frac{1}{\Delta\varepsilon_o}\left(S_o^{sat}\|\mathbf{P}\|\sin\phi_P - S_o\right)\dot{\lambda}, \quad S_o^{sat} = q_o R \tag{8}$$

The constant $q_o$ relates the maximal extra strength contribution to the isotropic hardening $R$ and $\Delta\varepsilon_o$ represents a strain scale for the transient cross hardening to take place. The initial value of $S_o$ is zero. The extra strength due to reversal or pseudo-reversal of the strain path is modeled by the scalar $S_r$, which evolves according to

$$\dot{S}_r = \frac{1}{\Delta\varepsilon_r}\left(-S_r^{sat}\min\left(\|\mathbf{P}\|\cos\phi_P, 0\right) - S_r\right)\dot{\lambda}, \quad S_r^{sat} = q_r R \tag{9}$$

The constant $q_r$ relates the maximal strength contribution due to the reverse SPC to the isotropic hardening, $\Delta\varepsilon_r$ controls the strain scale for $S_r$ to saturate. The initial value of $S_r$ is zero.

A two-term Voce hardening rule (Voce, 1948) is used for a precise modeling of the isotropic hardening and two extra terms are added to deal with SPC transients

$$\dot{R} = \sum_{i=1}^{2} \dot{R}_i + \left( h_r^{tr} + h_o^{tr} \right) \dot{\lambda} \tag{10}$$

where

$$\dot{R}_i = \frac{1}{\Delta \varepsilon_{R_i}} \left( R_i^{sat} - R_i \right) \dot{\lambda} \tag{11}$$

and

$$h_r^{tr} = k_r \min\left( \|\mathbf{P}\| \cos \phi_P, 0 \right), \quad h_o^{tr} = -k_o \|\mathbf{P}\| \sin \phi_P \tag{12}$$

The parameters $R_i^{sat}$ and $\Delta \varepsilon_{R_i}$ represent in turn the saturation value of the hardening variable $R_i$ and the strain scale for the saturation process. The initial yield stress is defined by giving $R$ an initial value $R_0$. The effects of SPCs involving reverse and orthogonal loading on the hardening rate are defined by the coefficients $k_r$ and $k_o$, respectively. A two-term Armstrong-Frederick rule (Armstrong and Frederick, 1966) is applied for the back stress

$$\mathbf{X} = \sum_{i=1}^{2} \mathbf{X}_i, \quad \dot{\mathbf{X}}_i = \frac{1}{\Delta \varepsilon_{X_i}} \left( X_i^{sat} \frac{\mathbf{S}'}{\bar{\sigma}(\bar{\varepsilon})} - \mathbf{X}_i \right) \dot{\lambda} \tag{13}$$

where $\mathbf{S}'$ is the deviatoric part of the overstress tensor, and the parameters $X_i^{sat}$ and $\Delta \varepsilon_{X_i}$ control the magnitude and strain scale of the two back stress tensors $\mathbf{X}_i$.

### 2.2 The modified HAH model

In order to improve the predictions of the HAH model, by accounting for hardening stagnation after reverse SPC and permanent softening after orthogonal SPC, some modifications are made here as compared to the formulation in Barlat et al. (2014). The HAH model is based on a positive homogeneous yield function of order one, which is regarded as the stable component, and which is combined with a fluctuating component. The fluctuating component consists of two hyperplanes in the deviatoric stress space with a common normal direction prescribed by the deviatoric tensor $\bar{\mathbf{h}}$, which is denoted the microstructure deviator as it memorizes the effect of the evolution history of the microstructure. The evolution equation for $\bar{\mathbf{h}}$

has the property that the magnitude of the tensor is conserved, and it is assumed here without loss of generality that $\left\|\bar{\mathbf{h}}\right\|=1$.

The yield criterion reads

$$f \equiv \Phi\left(\boldsymbol{\sigma}'\right)-\bar{\sigma}\left(\bar{\varepsilon}\right)=0 \tag{14}$$

where $\boldsymbol{\sigma}'$ is the deviatoric part of the stress tensor, $\bar{\sigma}$ is the flow stress, $\bar{\varepsilon}$ is the equivalent plastic strain, and the equivalent stress $\Phi\left(\boldsymbol{\sigma}'\right)$ is defined by

$$\Phi\left(\boldsymbol{\sigma}'\right)=\left(\left(\varphi^2\left(\boldsymbol{\sigma}'_A\right)+\varphi^2\left(\boldsymbol{\sigma}'_B\right)\right)^{q/2}+f_1^q\left(\tfrac{3}{8}\right)^{q/2}\left|\bar{\mathbf{h}}:\boldsymbol{\sigma}'-\left|\bar{\mathbf{h}}:\boldsymbol{\sigma}'\right|\right|^q+f_2^q\left(\tfrac{3}{8}\right)^{q/2}\left|\bar{\mathbf{h}}:\boldsymbol{\sigma}'+\left|\bar{\mathbf{h}}:\boldsymbol{\sigma}'\right|\right|^q\right)^{\frac{1}{q}} \tag{15}$$

with

$$\boldsymbol{\sigma}'_A=g_L^{-1}\boldsymbol{\sigma}'+\left(1-g_L^{-1}\right)\left(\bar{\mathbf{h}}:\boldsymbol{\sigma}'\right)\bar{\mathbf{h}},\quad \boldsymbol{\sigma}'_B=4\left(1-g_S\right)\left(\boldsymbol{\sigma}'-\left(\bar{\mathbf{h}}:\boldsymbol{\sigma}'\right)\bar{\mathbf{h}}\right) \tag{16}$$

The exponent $q$ is constant, while $g_L$ and $g_S$ are functions of the strain history. The yield function $\varphi$ is any positive homogeneous function of order one. The reverse hardening stagnation cannot be predicted by the enhanced HAH model. To account for this behavior, $f_1^q$ and $f_2^q$ are modified as follows

$$f_1^q=\frac{1}{\left(g_1+g_5\left(1-g_1\right)\right)^q}-1,\quad f_2^q=\frac{1}{\left(g_2+g_6\left(1-g_2\right)\right)^q}-1 \tag{17}$$

The evolution equations for the functions $g_1$ and $g_2$ are taken from Barlat et al. (2014). To enable use of a simple, phenomenological isotropic hardening rule, in the same manner as in the MHH model, the two extra functions $g_5$ and $g_6$ are added to model the observed hardening stagnation after reverse SPC. The modification of the HAH model is an alternative to the dislocation based work hardening model (Rauch et al., 2007) which was used by Barlat et al., (2011). Note that the enhanced HAH model is obtained by setting $g_5=g_6=0$. Evolution equations for the $g$ functions will be defined below.

The plastic rate-of-deformation tensor is defined by the associated flow rule in the form

$$\mathbf{D}^p=\dot{\lambda}\frac{\partial\Phi\left(\boldsymbol{\sigma}'\right)}{\partial\boldsymbol{\sigma}} \tag{18}$$

where $\dot{\lambda}$ is still the plastic multiplier. The equivalent plastic strain $\bar{\varepsilon}$ is defined by Equation (5). The microstructural stress tensor $\bar{\mathbf{h}}$ evolves as (Barlat et al., 2014)

$$\frac{d\bar{\mathbf{h}}}{d\bar{\varepsilon}} = k\,\mathrm{sign}\left(\cos\chi\right)\left(\left|\cos\chi\right|^{1/z} + g_R\right)\left(\frac{\boldsymbol{\sigma}'}{\|\boldsymbol{\sigma}'\|} - \bar{\mathbf{h}}\cos\chi\right) \tag{19}$$

where $k$ and $z$ are constants, $g_R$ is a function, and further

$$\cos\chi = \frac{\boldsymbol{\sigma}'}{\|\boldsymbol{\sigma}'\|} : \bar{\mathbf{h}} \tag{20}$$

For a well annealed material, the initial direction of $\bar{\mathbf{h}}$ is not defined, since no direction can be distinguished from any others. Apparently, this makes the model mathematically ill-posed, but the problem was overcome by Barlat et al. (2011) by taking the initial direction of $\bar{\mathbf{h}}$ equal to the direction of the deviatoric stress tensor during the first plastic strain increment. Since the functions $g_1$ and $g_2$ initially are equal to unity for a well annealed material, the fluctuating part of the yield surface vanishes and the degenerated problem can be solved to give the first plastic strain increment without knowing the initial value of $\bar{\mathbf{h}}$. As is evident from Equation (19), the microstructure deviator $\bar{\mathbf{h}}$ always rotates in the half-plane, towards the direction collinear with the current deviatoric stress direction.

The evolution equations for the $g$ functions are defined as

$$\frac{dg_R}{d\bar{\varepsilon}} = k_R\left(k'_R\left(1-\cos^2\chi\right) - g_R\right) \tag{21}$$

$$\frac{dg_L}{d\bar{\varepsilon}} = k_L\left(\frac{\bar{\sigma}\left(\bar{\varepsilon}\right)-\bar{\sigma}\left(0\right)}{\bar{\sigma}\left(\bar{\varepsilon}\right)}\left(\sqrt{L\left(1-\cos^2\chi\right)+\cos^2\chi}-1\right)+1-g_L\right) \tag{22}$$

$$\frac{dg_S}{d\bar{\varepsilon}} = k_S\left(1+\left(S-1\right)\cos^2\chi - g_S\right) \tag{23}$$

$$\frac{dg_1}{d\bar{\varepsilon}} = \begin{cases} k_2\left(k_3\dfrac{\bar{\sigma}\left(0\right)}{\bar{\sigma}\left(\bar{\varepsilon}\right)} - g_1\right) & \text{if } \bar{\mathbf{h}}:\boldsymbol{\sigma}' \geq 0 \\ k_1\dfrac{g_4 - g_1}{g_1} & \text{if } \bar{\mathbf{h}}:\boldsymbol{\sigma}' < 0 \end{cases} \tag{24}$$

$$\frac{dg_2}{d\bar{\varepsilon}}=\begin{cases} k_1\dfrac{g_3-g_2}{g_2} & \text{if } \bar{\mathbf{h}}:\boldsymbol{\sigma}'\geq 0 \\ k_2\left(k_3\dfrac{\bar{\sigma}(0)}{\bar{\sigma}(\bar{\varepsilon})}-g_2\right) & \text{if } \bar{\mathbf{h}}:\boldsymbol{\sigma}'<0 \end{cases} \tag{25}$$

$$\frac{dg_3}{d\bar{\varepsilon}}=\begin{cases} 0 & \text{if } \bar{\mathbf{h}}:\boldsymbol{\sigma}'\geq 0 \\ k_5\left(k_4-g_3\right) & \text{if } \bar{\mathbf{h}}:\boldsymbol{\sigma}'<0 \end{cases} \tag{26}$$

$$\frac{dg_4}{d\bar{\varepsilon}}=\begin{cases} k_5\left(k_4-g_4\right) & \text{if } \bar{\mathbf{h}}:\boldsymbol{\sigma}'\geq 0 \\ 0 & \text{if } \bar{\mathbf{h}}:\boldsymbol{\sigma}'<0 \end{cases} \tag{27}$$

$$\frac{dg_5}{d\bar{\varepsilon}}=\begin{cases} 0 & \text{if } \bar{\mathbf{h}}:\boldsymbol{\sigma}'\geq 0 \\ k_7\left(-\dfrac{k_6}{k_2}\dfrac{dg_2}{d\bar{\varepsilon}}-g_5\right) & \text{if } \bar{\mathbf{h}}:\boldsymbol{\sigma}'<0 \end{cases} \tag{28}$$

$$\frac{dg_6}{d\bar{\varepsilon}}=\begin{cases} k_7\left(-\dfrac{k_6}{k_2}\dfrac{dg_1}{d\bar{\varepsilon}}-g_6\right) & \text{if } \bar{\mathbf{h}}:\boldsymbol{\sigma}'\geq 0 \\ 0 & \text{if } \bar{\mathbf{h}}:\boldsymbol{\sigma}'<0 \end{cases} \tag{29}$$

where $L$, $S$, $k_L$, $k_S$, $k_R$, $k_R'$ and $k_1,...,k_7$ are constants and further $\bar{\sigma}(0)$ is the initial yield stress. For a well annealed material, the initial values of $g_L$, $g_S$ and $g_1,...,g_4$ are unity, while $g_R$, $g_5$ and $g_6$ are initially zero. The magnitude of $dg_2/d\bar{\varepsilon}$ and $dg_1/d\bar{\varepsilon}$ starts from a very high value and then gradually decreases when the sign of $\bar{\mathbf{h}}:\boldsymbol{\sigma}'$ is changed to be smaller and larger than zero, respectively. Thus, the functions $g_5$ and $g_6$ start from zero and then increase to a high value before they gradually decrease towards zero. During preloading, $g_6$ will not affect the stress-strain curve because $g_2$ remains equal to unity. The function $g_5$ provides hardening stagnation after reverse SPC, while $g_6$ contributes after double reverse SPC.

Either the Swift hardening rule or the two-term Voce hardening rule is adopted to describe isotropic hardening in the HAH model. In order to capture the permanent softening behavior after orthogonal SPCs, an extra hardening term is included in the isotropic hardening rule. In the first case, the hardening rule is expressed as

$$\dot{\bar{\sigma}}=Cn\left(\varepsilon_0+\bar{\varepsilon}\right)^{n-1}\dot{\lambda}+h_o^{tr}\dot{\lambda} \tag{30}$$

where $C$, $n$ and $\varepsilon_0$ are constants; in the second case, the hardening rule reads

$$\dot{\bar{\sigma}} = \sum_{i=1}^{2} \dot{R}_i + h_o^{tr} \dot{\lambda} \tag{31}$$

with $\dot{R}_i$ defined by Equation (11). The last term in Equations (30) and (31) is included to describe permanent softening subsequent to an orthogonal SPC. The modulus $h_o^{tr}$ is defined by

$$h_o^{tr} = -k_o \sin \chi \tag{32}$$

where $k_o$ is a constant. Subsequent to an orthogonal SPC, the modulus $h_o^{tr}$ fades away as the microstructure deviator becomes parallel with the current deviatoric stress tensor, i.e., as $\sin \chi$ approaches zero. Consequently, a permanent softening of the flow stress will be obtained. Note that the original model by Barlat et al. (2014) is obtained by setting $h_o^{tr} = 0$.

## 3. Parameter identification and simulation results

The HAH model is calibrated using experimental data for commercially pure aluminum and EDDQ steel. The identification procedure used in Barlat et al. (2014) is employed. For the MHH model, the parameter set identified by Mánik et al. (2015) was applied for commercially pure aluminum, while a similar calibration procedure as used by Mánik et al. (2015) was performed to obtain parameters for EDDQ steel. The two-term Voce hardening rule gave a similarly good fit as the Swift hardening rule to the monotonic stress-strain curve of this material.

The parameter set of the HAH model determined by Lee et al. (2015) based on the experiments presented by Ha et al. (2013) was adopted for EDDQ steel with two exceptions. The parameters $k_L$ and $k$ were slightly changed by including all tensile directions reported by Ha et al. (2013) for the second strain path. Lee et al. (2015) used only the tensile test in the 45° direction in their parameter identification. Owing to the lack of reversal tests for EDDQ steel and the experimental observation that this material does not exhibit permanent softening after orthogonal SPCs, the extra functions $g_5$, $g_6$ and $h_o^{tr}$ were not employed. This can formally be achieved by setting $k_6$, $k_7$ and $k_o$ equal to zero. In the case of commercially pure aluminum, a similar calibration of the parameters as for the EDDQ steel was performed, but an additional

iteration was made to determine the new parameters $k_6$, $k_7$ and $k_o$, so that details of the reverse hardening stagnation and orthogonal permanent softening could be better described.

### 3.1. Commercially pure aluminum

In Mánik et al. (2015), isotropic sheets of commercially pure aluminum, cut by spark erosion from an as-cast billet, were applied to perform tensile tests prestrained by either compression or rolling to study the Bauschinger effect and the cross-hardening effect, respectively. The Hershey yield function (Hershey, 1954) with exponent of 8 is used for both the MHH and HAH models, since the commercial pure aluminum was initially isotropic. The calibrated coefficients of the HAH model using the two-term Voce hardening rule, are listed in **Table 1**. As the material did not exhibit orthogonal softening, $k_s = 0$ provided the best agreement with the experimental data. The parameter set used for the MHH model is given by Mánik et al. (2015).

**Table 1**. Model parameters for commercially pure aluminum

| HAH model | | | | | | | | | | | |
|---|---|---|---|---|---|---|---|---|---|---|---|
| $m$ | $q$ | $\bar{\sigma}(0)$ | $R_1^{sat}$ | $\Delta\varepsilon_{R_1}$ | $R_2^{sat}$ | $\Delta\varepsilon_{R_2}$ | $k_1$ | $k_2$ | $k_3$ | $k_4$ | $k_5$ |
| [–] | [–] | [MPa] | [MPa] | [–] | [MPa] | [–] | [–] | [–] | [–] | [–] | [–] |
| 8 | 2 | 13.39 | 62.5 | 0.17 | 25.79 | 0.0165 | 30 | 200 | 0.8 | 0.63 | 5.0 |
| $k_6$ | $k_7$ | $k_o$ | $k_L$ | $L$ | $k_S$ | $S$ | $k$ | $z$ | $k_R$ | $k'_R$ | |
| [–] | [–] | [–] | [–] | [–] | [–] | [–] | [–] | [–] | [–] | [–] | |
| 7.5 | 40 | 50 | 1000 | 1.15 | 0 | 0 | 25 | 5 | 15 | 0.20 | |

**Fig. 1** shows the experimental and simulated stress-strain curves from tensile tests in different directions after prestraining by rolling. The tensile direction is defined with respect to the rolling direction. In addition, the experimental and simulated tensile stress-strain curves of the as-cast material are presented. The experimental results show that commercially pure aluminum exhibits stress overshooting and permanent softening after orthogonal SPCs. It is evident that the MHH model captures the stress overshooting and permanent softening as

function of tensile direction. An exception is the stress overshooting in the 0° direction after a prestrain of 8% which is overestimated. The HAH model captures the stress overshooting and permanent softening in the 90° direction after prestrains of 5% and 9%, while the stress overshooting is underestimated for the tensile tests in the 0°, 30° and 50° directions after 8% prestrain.

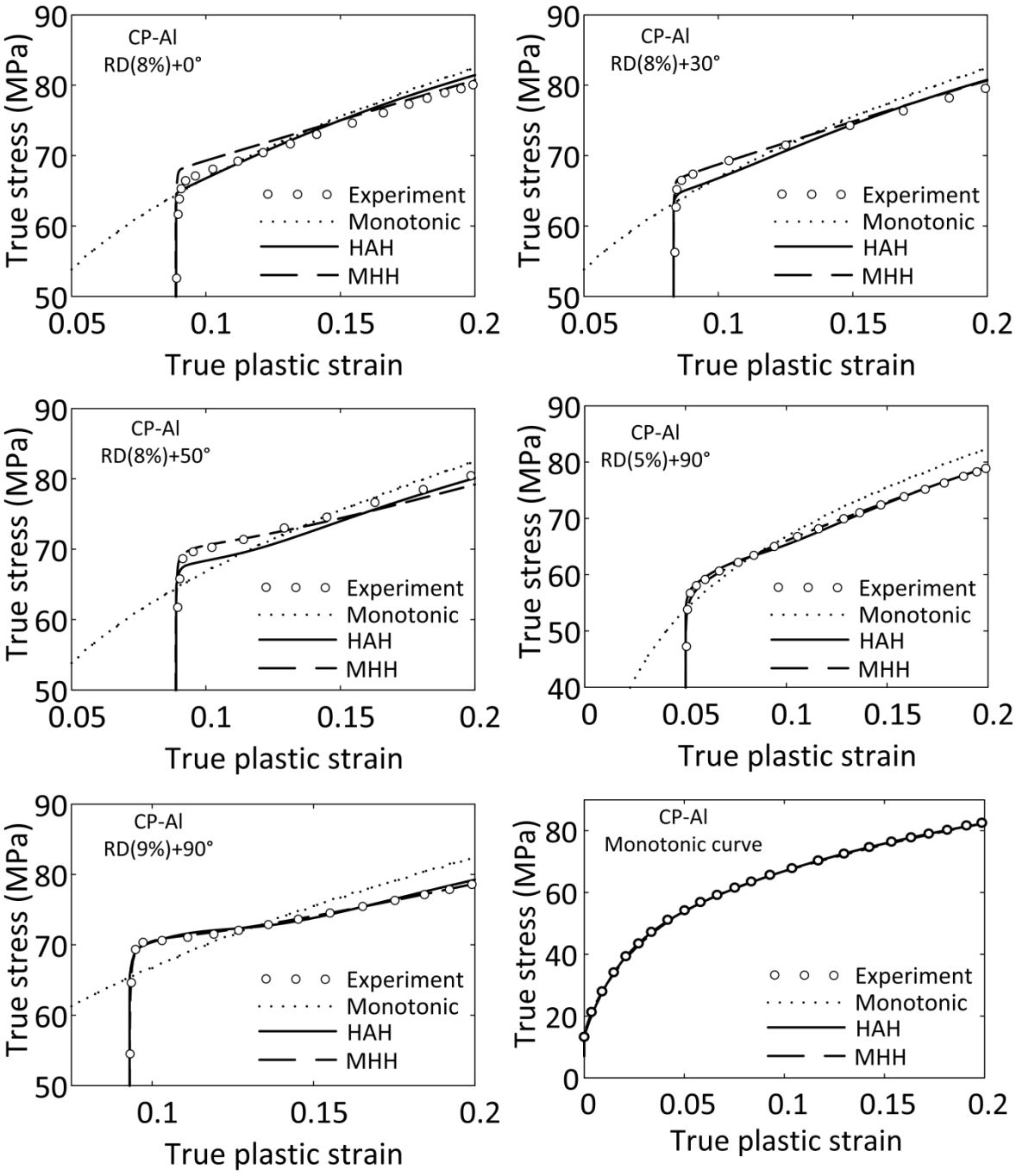

**Fig. 1**. Experimental and simulated stress-strain curves for commercially pure aluminum (CP-Al) from tensile tests in different directions subsequent to prestraining by rolling and tensile tests of the as-cast material.

**Fig. 2** presents the stress-strain curves from tensile tests after prestraining in compression to 2% and 4.4% along with the stress-strain curve for monotonic loading. After the strain reversal, the stress-strain curves exhibit reverse softening and hardening stagnation, and permanent softening is observed in the strain range investigated. The calculation of the initial yield stress is acceptable for both models, even though the stress levels are slightly different. Due to the rapid initial hardening, it is difficult to judge experimentally exactly when the material starts to yield during reverse loading. With the modifications of the HAH model it can, in the same way as the MHH model, successfully reproduce not only the Bauschinger effect, but also the hardening stagnation and the permanent softening effect during reverse SPC.

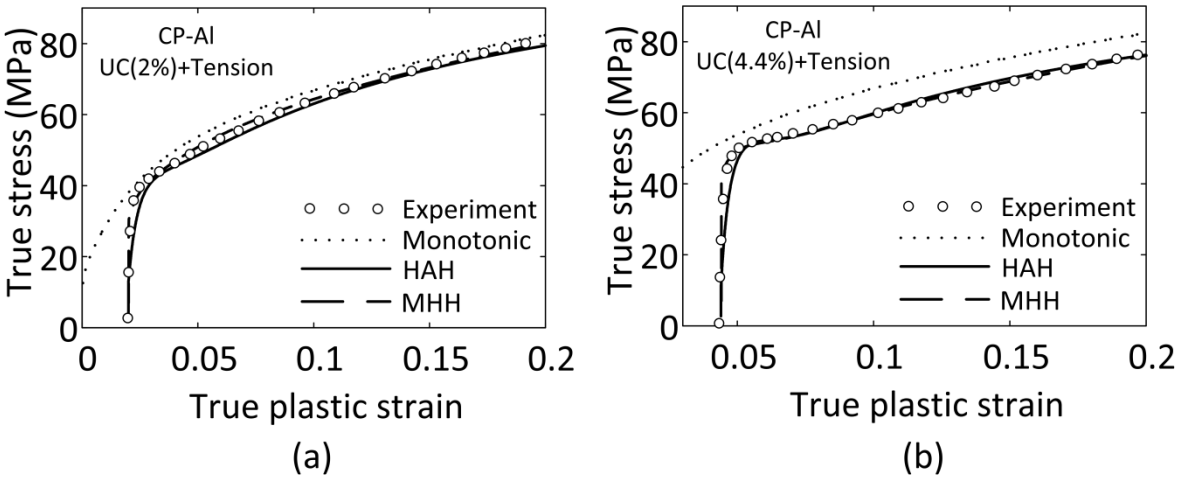


**Fig. 2**. Experimental and simulated stress-strain curves for commercially pure aluminum (CP-Al) from tensile tests after prestraining by uniaxial compression (UC) to (a) 2% and (b) 4.4% together with the stress-strain curve for monotonic loading.

The R-value is defined as the width-to-thickness strain-rate ratio in uniaxial tension and can be calculated from the gradient of the yield surface. Without predeformation the R-value normally changes little during monotonic loading. However, subsequent to an orthogonal SPC a transient rapid variation was reported by Mánik et al. (2015) for the commercial pure aluminum alloy. **Fig. 3** presents the experimental evolution and corresponding simulation of the R-value in

a tensile test in the 90° direction subsequent to 5% prestraining by rolling. This corresponds to an orthogonal SPC. The variation of the R-value is due to the microstructurally induced transient behavior subsequent to the orthogonal SPC. It is evident that only the MHH model is capable of describing the experimental evolution of the R-value with good accuracy.

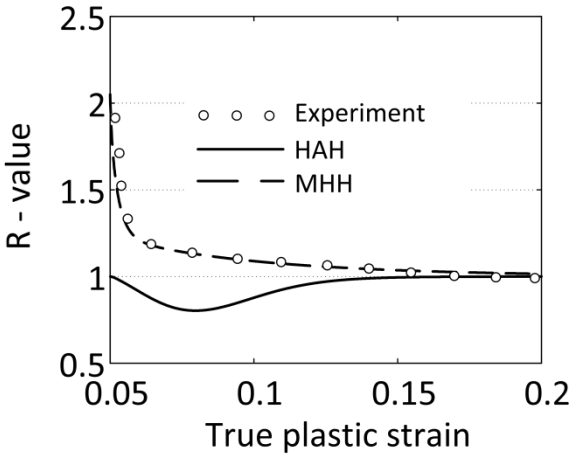


**Fig. 3**. Experimental and simulated evolution of the R-value with straining for commercially pure aluminum based on a tensile test in the transverse direction after a prestrain of 5% by rolling.

The evolution of the yield surface of the MHH and HAH models is illustrated in **Fig. 4** for commercially pure aluminum. **Fig. 4**a shows the evolution during a tension test in the rolling direction. Kinematic hardening shifts the yield surface of the MHH model in the loading direction as compared to an isotropically expanding yield surface, which is included for comparison. The HAH model, on the other hand, distorts the yield surface by compressing and flattening it in the direction opposite to the tensile direction.

The preloading by rolling in the *x*-direction in **Fig. 4**b has shifted the yield surface of the MHH model in the *x*-direction. Subsequently, the tensile test in the orthogonal *y*-direction starts shifting the yield surface mainly in the *y*-direction, but also in the negative *x*-direction, as the back stress tensor adapts to the second strain path. The influence of the prerolling on the yield surface of the HAH model is significant flattening in the negative *x*-direction. Subsequent to the SPC, this distorted and flattened part starts rotating counter-clockwise towards the direction defined by the second strain path.

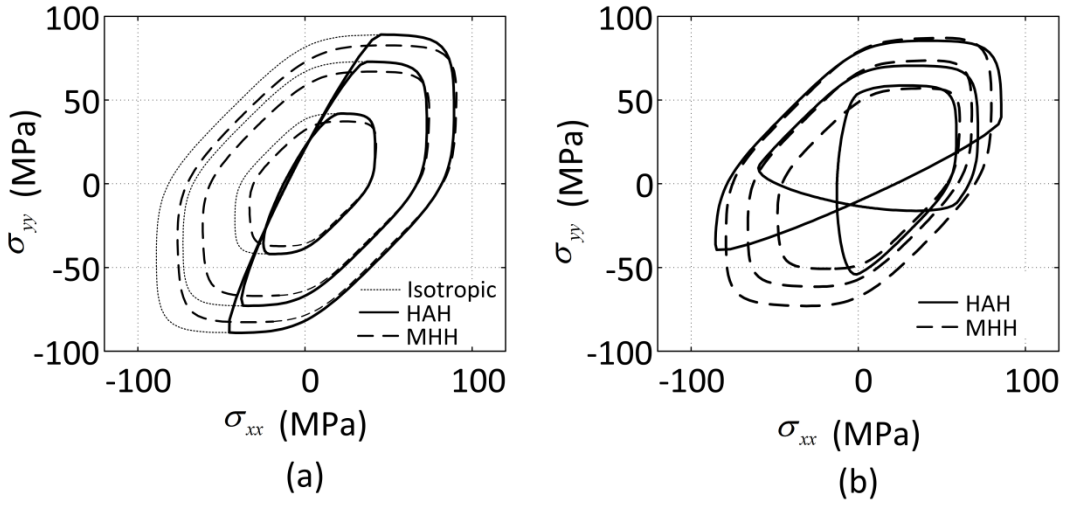


**Fig. 4**. Evolution of the yield surface of the MHH and HAH models for commercially pure aluminum: (a) uniaxial tension in the rolling direction (*x*-direction) and (b) uniaxial tension in the transverse direction (*y*-direction) subsequent to 5 % prestraining by rolling in the *x*-direction. The yield surfaces are plotted for equivalent plastic strains equal to 5 %, 10 % and 19.5 %.

**Fig. 5** illustrates, in the π-plane, the rotation of the microstructure deviator tensors of the two models for the same loading sequence as in **Fig. 4**b, namely 5% prestraining by rolling in the *x*-direction followed by uniaxial tension in the *y*-direction. Each arrow corresponds to a specific equivalent plastic strain. Prior to the SPC the directions of the microstructure deviator tensors remain paralell. These arrows are shifted slightly from the origin so that they can be distinguished in the figure. During prerolling, the microstructure deviator tensor $\bar{\mathbf{h}}$ keeps its direction and magnitude, whereas $\mathbf{P}$ starts from zero magnitude and gradually grows in the direction defined by the rolling. As the strain path is changed to uniaxial tension in the *y*-direction, $\bar{\mathbf{h}}$ rotates but never changes its magnitude, while $\mathbf{P}$ rotates with a simultanious change of its magnitude, taking the shortest route towards its new saturated state.

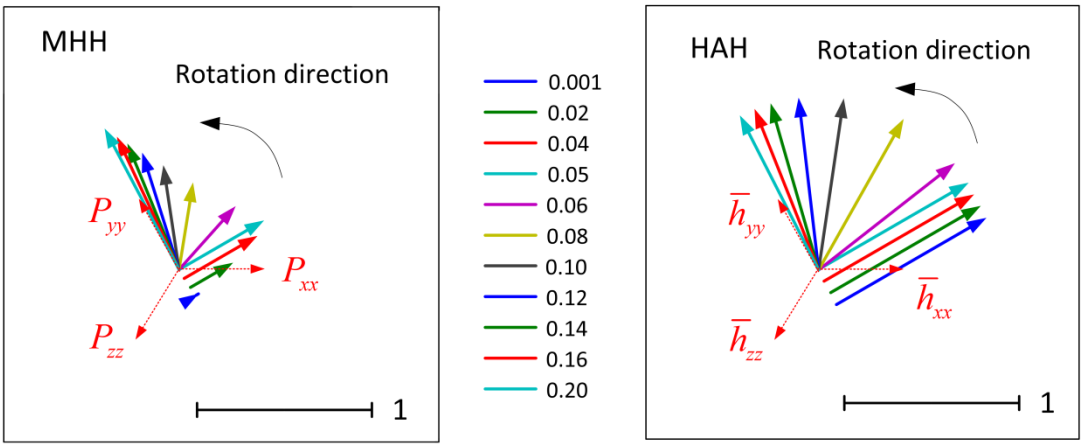


**Fig. 5**. Magnitude and direction of the microstructure deviator tensors **P** and $\bar{\mathbf{h}}$ used in the MHH and HAH models, respectively, during 5% prestraining by rolling in the *x*-direction followed by uniaxial tension in the *y*-direction. The initial parallel tensors are shifted to make it possible to distinguish them in the figure.

### 3.2. EDDQ steel

Stress-strain curves of the EDDQ steel in uniaxial tension at various directions after prestraining have been reported by Ha et al. (2013). The HAH model has earlier been calibrated to some of these experiments by Lee et al. (2015) and with a slightly improved calibration made here, as described above. The difference between the two calibrations of the HAH model is that the transient after a SPC lasts slightly longer in the simulations using the new parameter set, as illustrated in **Fig. 6** for one of the tests used in the calibration. Note that the improved calibration preserves the same level of accuracy for the stress-strain curves considered by Lee et al. (2015). The Yld2000-2d yield function (Barlat et al., 2003) with exponent of 6 and coefficients from Lee et al. (2015) was used for EDDQ steel in both the MHH and HAH models. The remaining parameters identified for the MHH and HAH models are listed in **Table 2**. The two-term Voce hardening rule is selected for the MHH model, while as in the calibration by Lee et al. (2015), the Swift hardening rule is applied for the HAH model. Owing to the lack of experimental data for the Bauschinger effect of the EDDQ steel, kinematic hardening was not employed in this calibration of the MHH model. Furthermore, the material did not exhibit orthogonal softening, hence $k_s = 0$ provided the best calibration.

**Table 2** Model parameters for EDDQ steel

| HAH model | | | | | | | | | | | |
|---|---|---|---|---|---|---|---|---|---|---|---|
| $m$ | $q$ | $C$ | $\varepsilon_0$ | $n$ | $k$ | $k_o$ | $k_1$ | $k_2$ | $k_3$ | $k_4$ | $k_5$ |
| [–] | [–] | [MPa] | [–] | [–] | [–] | [–] | [–] | [–] | [–] | [–] | [–] |
| 6 | 2 | 538.0 | 0.0075 | 0.267 | 14 | 0 | 880.0 | 63.0 | 0.64 | 1.0 | 0.0 |
| $k_6$ | $k_7$ | $k_L$ | $L$ | $k_S$ | $S$ | $z$ | $k_R$ | $k'_R$ | | | |
| [–] | [–] | [–] | [–] | [–] | [–] | [–] | [–] | [–] | | | |
| 0 | 0 | 500 | 1.65 | 0 | 0 | 5 | 15 | 0.20 | | | |

| MHH model | | | | | | | | | | | |
|---|---|---|---|---|---|---|---|---|---|---|---|
| $m$ | $R_0$ | $R_1^{sat}$ | $\Delta\varepsilon_{R_1}$ | $R_2^{sat}$ | $\Delta\varepsilon_{R_2}$ | $X_1^{sat}$ | $\Delta\varepsilon_{X_1}$ | $X_2^{sat}$ | $\Delta\varepsilon_{X_2}$ | $\Delta\varepsilon_P$ | $\Delta\varepsilon_o$ |
| [–] | [MPa] | [MPa] | [–] | [MPa] | [–] | [MPa] | [–] | [MPa] | [–] | [–] | [–] |
| 6 | 150 | 323 | 0.5 | 97 | 0.04 | 0 | – | 0 | – | 0.05 | 0.002 |
| $\Delta\varepsilon_r$ | $q_0$ | $q_r$ | $k_0$ | $k_r$ | | | | | | | |
| [–] | [–] | [–] | [MPa] | [MPa] | | | | | | | |
| 0.05 | 0.18 | 0.2 | 0 | 0 | | | | | | | |

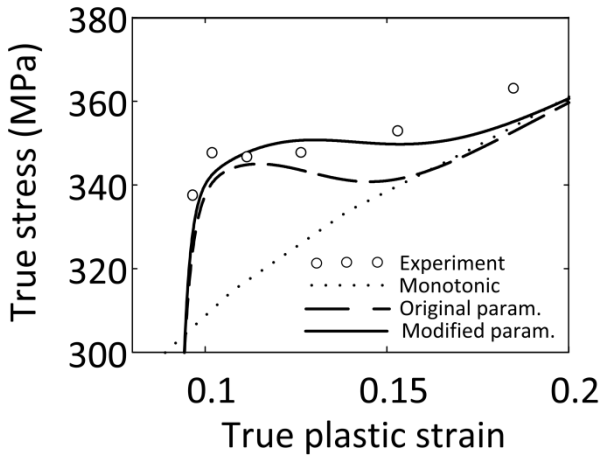


**Fig. 6**. Experimental and simulated stress-strain curves for EDDQ steel in uniaxial tension in the 60° direction after 10 % prestraining by uniaxial tension along RD, using the original and new parameter sets for the HAH model.

The experimental and simulated stress-strain curves for monotonic, uniaxial tension and uniaxial tension in various directions subsequent to 4 % and 10 % prestraining in tension along RD are presented in **Fig. 7** - **Fig. 9**. As shown in **Fig. 7**, both models are capable of representing the monotonic stress-strain curve. The simulations of the stress-strain curves after 4 % prestraining are similar and mostly in agreement with the experimental results, see **Fig. 8**. Larger differences are found between the experimental and simulated stress-strain curves after 10 % prestrain in **Fig. 9**. Owing to the higher prestrain level, the stress overshoots are markedly larger than in **Fig. 8**. It is evident from **Fig. 9** that the MHH model is in better agreement with the experiments than the HAH model, which is only able to capture the stress overshoot in the 45° and 60° tensile tests. In the other directions, the HAH model underestimates the stress overshoot.

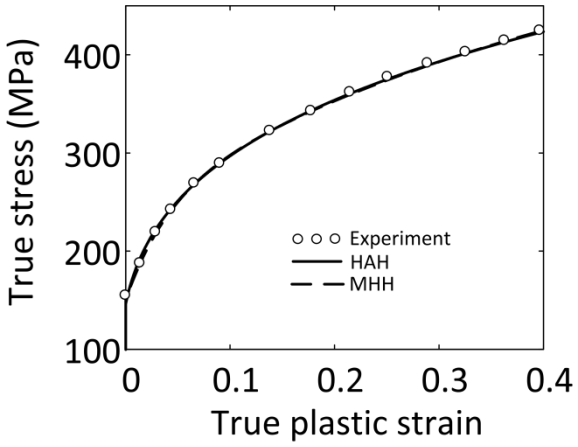


**Fig. 7**. Monotonic stress-strain curve in uniaxial tension along RD for EDDQ steel.

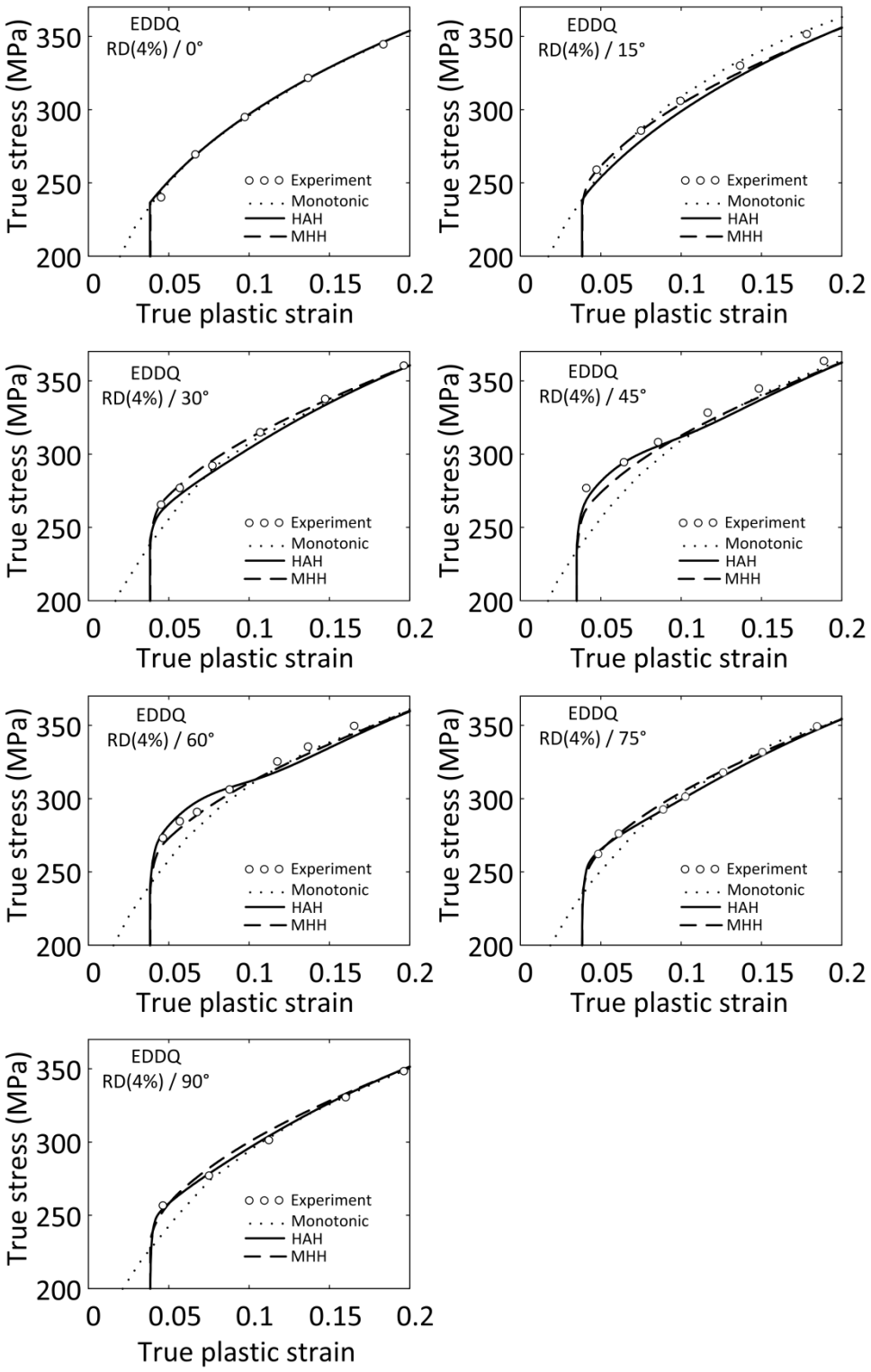


**Fig. 8**. Stress-strain curves in uniaxial tension at various direction with respect to RD after 4 % prestraining in uniaxial tension along RD for EDDQ steel.

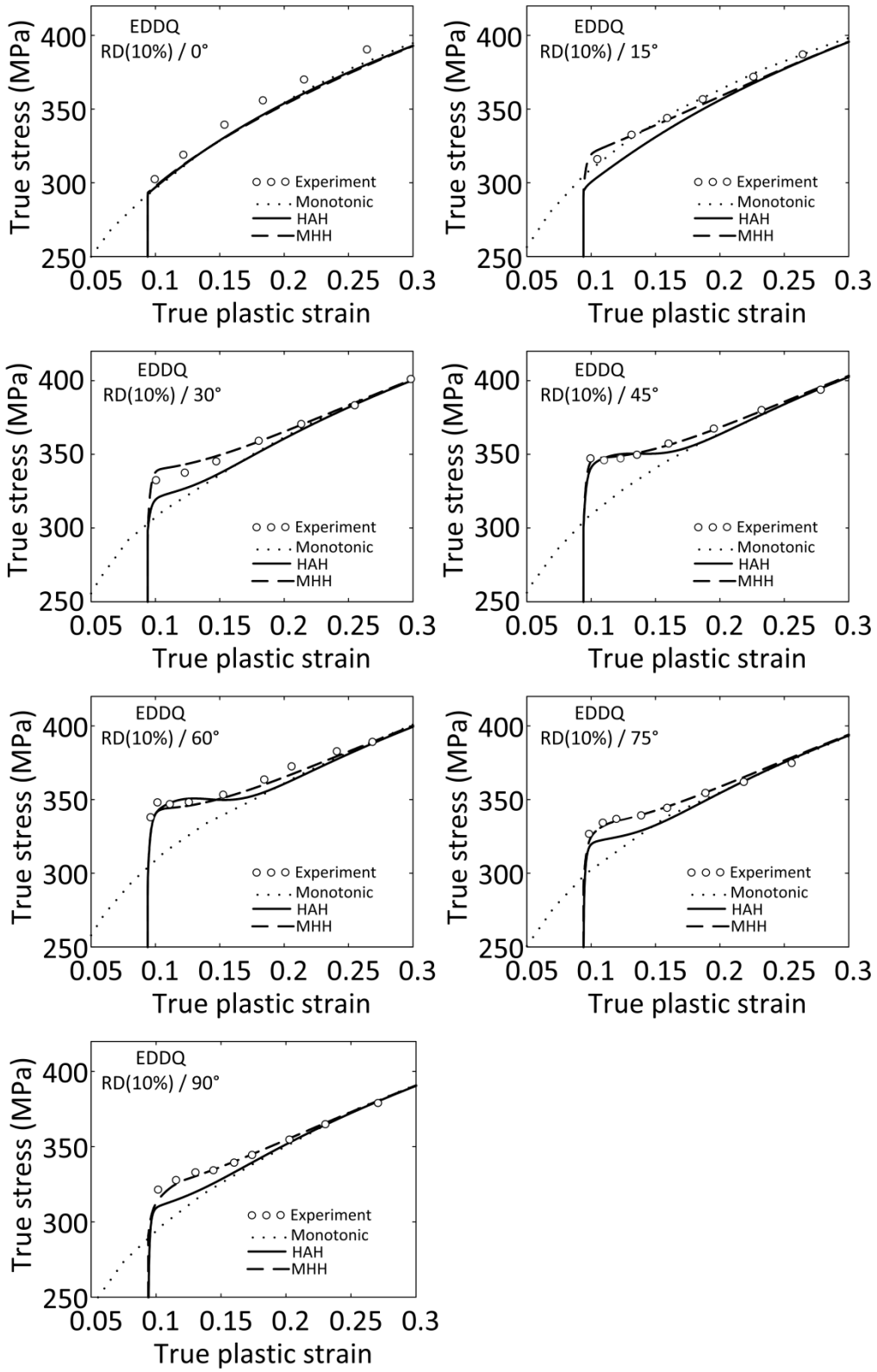


**Fig. 9**. Stress-strain curves in uniaxial tension at various direction with respect to RD after about 10 % prestraining in uniaxial tension along RD for EDDQ steel.

Simulations of double SPCs were made with the two models based on the parameters for EDDQ steel. Experimental data for double SPCs is lacking. The orthogonal distortion of the yield surface introduced into the HAH model by Barlat et al. (2014) was designed to qualitatively agree with the experimentally observed behavior of a low carbon steel reported by Vincze et al. (2013). The results from simulations of double SPCs are presented in **Fig. 10**. The loading sequence consists of uniaxial tension along RD, followed by uniaxial tension along the 45° direction and finally uniaxial tension along RD. The straining between the first and second SPC is varied. When the second SPC occurs early during the transient of the first SPC, see **Fig. 10**a, the HAH model will nearly return to the monotonic stress-strain curve in uniaxial tension along RD. Even when the second SPC occurs at a later stage of the transient of the first SPC, as in **Fig. 10**b, the HAH model almost returns to the monotonic stress-strain curve. A significant stress overshoot is only obtained when the second SPC takes place during the final stages of the transient after the first SPC, see **Fig. 10**c. Since the yield surface of the MHH model is not distorted, it starts from its expanded state during the transient of the first SPC. When the second SPC is made early in the transient, as in **Fig. 10**a, the yield surface rapidly shrinks from a higher stress level than the monotonic stress-strain curve, which is only approached after a prolonged transient. In the two other cases, see **Fig. 10**b and c, for which the second SPC occurs at a later stage, the MHH model responds with a new overshooting caused by the memory of the first SPC. It is seen that the MHH model predicts a qualitatively different behavior than the HAH model and thereby it differs from the behavior observed for low carbon steel by Vincze et al. (2013).

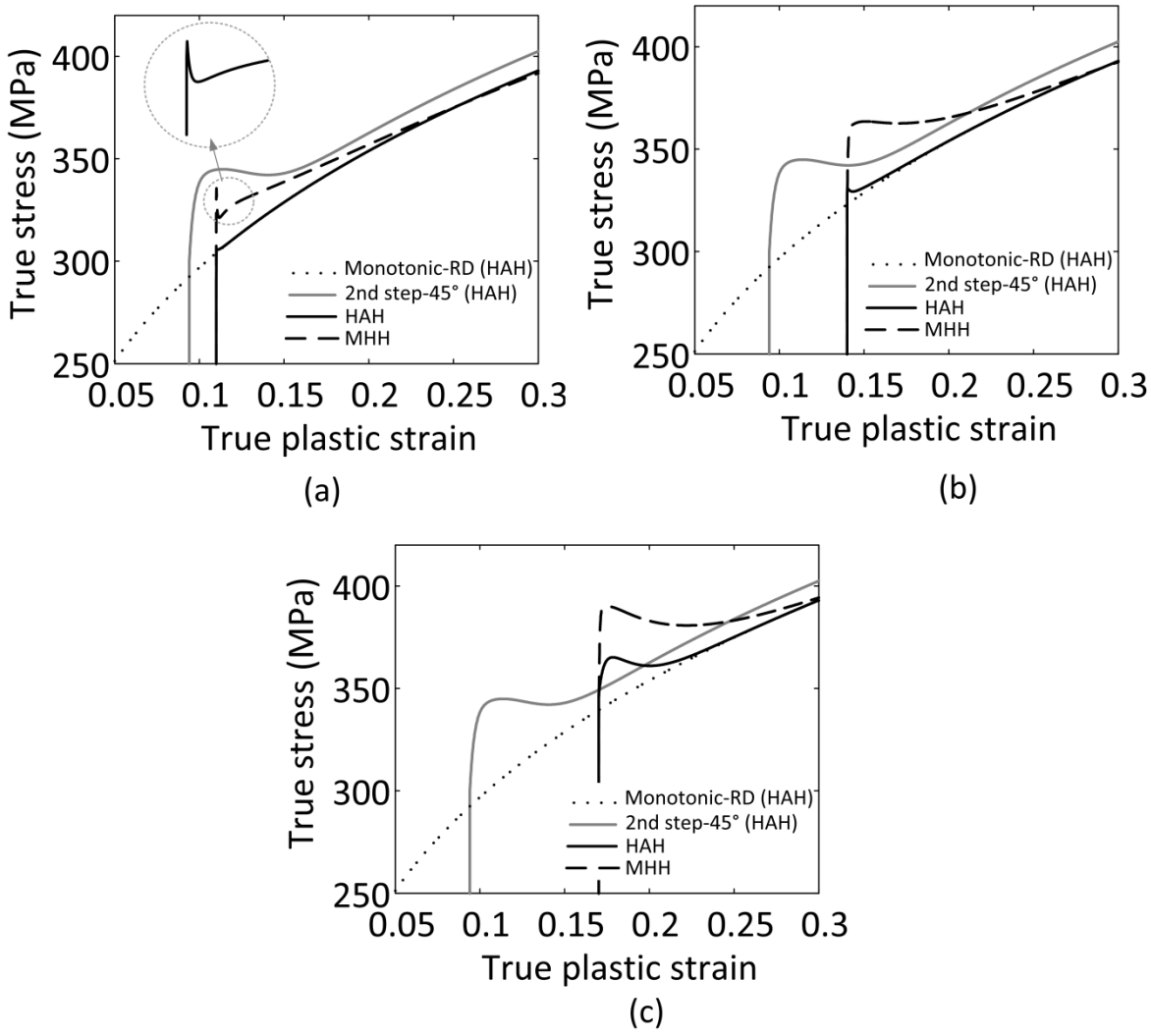


**Fig. 10**. Simulated double SPCs for EDDQ steel. The sub-figures present simulated stress-strain curves in monotonic, uniaxial tension along RD and in uniaxial tension along the 45° direction with tensile prestraining along RD. These two curves are obtained with the HAH model. The simulated stress-strain curves in uniaxial tension along RD after prestraining in tension first along RD and then along the 45° direction, are obtained by both models. The straining of the second step along the 45° direction increases from (a) to (c).

## 4. Discussion

The HAH and MHH models are phenomenological models designed to capture transients that occur subsequent to changes in the strain path. The material has a short-term memory of its previous strain path, which is described mathematically in terms of differential equations. This fading memory is by both models obtained by a microstructure deviator, namely $\mathbf{P}$ in the MHH model and $\bar{\mathbf{h}}$ in the HAH model, which is a second-order symmetric deviatoric tensor with five corresponding differential equations describing its evolution. In this work, the MHH model applies two back stress tensors $\mathbf{X}_i$ adding five coupled scalar differential equations each to be integrated. In many cases, one back stress tensor is sufficient to provide a satisfactory description. Furthermore, the MHH model has two more differential equations describing the expansion of the yield surface due to the extra strength contributions after SPCs, represented by the internal variables $S_0$ and $S_r$. In total, this amounts to 17 extra scalar equations to integrate for the case of commercially pure aluminum in addition to the isotropic hardening rule. Similarly there are 12 extra scalar differential equations in the HAH model for this alloy. The added computational cost related to solving these extra scalar differential equations is only a few times higher than the additional cost of applying a kinematic hardening model, which adds five differential equations per back stress tensor. Hence, the computational cost does not prevent industrial applications of such models. It is mentioned that the HAH model may suffer from numerical challenges when calculating purely orthogonal SPCs, because the local curvature of the yield surface may become large, which will delay or even destabilize the iteration process of the return map.

A more important issue impeding industrial applications is the complex calibration procedure of the significant number of model parameters that comes in addition to the basic parameters describing the monotonic stress-strain curve and the initial shape of the anisotropic yield surface. The HAH model has the advantage that the basic description is not altered by the additional equations added to model SPC effects. In contrast, the kinematic hardening contributes to the monotonic stress-strain curve in the MHH model, which means that the parameters governing isotropic and kinematic hardening have to be calibrated together. Provided a sufficient number of adequate mechanical tests are available, the calibration requires a non-linear minimization of the error. Such a calibration depends on how the measure of the error with

respect to the experiments is defined and weighted, and the solution may not be unique. A good calibration depends on a decent first guess of the parameters. The equations and the corresponding parameters of the MHH model have more straightforward interpretations in terms of experimental observations. The constitutive equations of the MHH model are simple first-order differential equations with well-defined strain scale parameters and stress saturation terms, for which a first guess can be reasonably estimated based on visual inspection of the stress-strain curves. In practice, it is important to inspect that all calibration experiments are matched satisfactorily after such a complex calibration.

The chief challenge for industrial applications is the added number of mechanical tests required for calibration and their complexity. In many applications with plates or sheets, reverse tensile tests are possible to perform only for very small tensile specimens with a length that equals a few times the thickness in order to avoid buckling. Alternatively, techniques with sideways support to avoid buckling during compression have been suggested (Boger et al., 2005; Yoshida et al., 2002) but are difficult to perform. An alternative is reverse simple shear tests, but for anisotropic materials these are more complex to analyze, since the transverse normal stress is not measured. Two-step tests for other SPCs with lower Schmitt angles may be obtained by pre-deformation; either by a large tensile specimen or by rolling in various directions. Anyhow, a rather large test matrix is required, and limited data are available, as of today few alloys have been systematically tested.

The microstructure deviator $\mathbf{P}$ in the MHH model is defined in the strain-rate space, while the counterpart $\bar{\mathbf{h}}$ in the HAH model is defined in the deviatoric stress space. While $\mathbf{P}$ can point in any direction during the forming process, $\bar{\mathbf{h}}$ can only change direction in a half plane. The corresponding Schmitt angles, which are used to quantify any abrupt SPC, are based on SPCs in these two spaces, respectively. A comparison of the two definitions is provided by Holmedal et al. (2008) and Mánik et al. (2015). In the case of prestrain in uniaxial tension followed by uniaxial tension in another material direction, the Schmitt angle defined in strain-rate space depends on the R-values of the two tensile tests, whereas the Schmitt angle defined in the deviatoric stress space does not. The EDDQ steel has a high R-value, about 2.5 in the rolling direction. If the EDDQ steel is prestrained by uniaxial tension in the rolling direction and then subjected to uniaxial tension in another direction $\alpha$ with respect to the rolling direction, the

Schmitt angle will be 90° (orthogonal) near $\alpha$ equal to 45° and 55° when measured in the strain-rate space and deviatoric stress space, respectively.

The amount of cross hardening can be quantified as the maximum stress overshoot, which is here defined as the maximum ratio between the flow stress after the SPC and the flow stress during monotonic straining at the same equivalent plastic strain. The maximum stress overshoot obtained with the two models during a SPC defined by prestraining to 9.4 % by uniaxial tension in the RD followed by uniaxial tension in a material direction $\alpha$ with respect to RD for EDDQ steel is shown in **Fig. 11**a. Since the R-value is large, the two models predict different variation of the stress overshoot with the angle $\alpha$, due to the different definitions of the microstructure deviator. In **Fig. 11**b, the predictions obtained by the two models are compared with the experimental findings reported by Ha et al. (2013) for EDDQ steel, where the stress overshoot is taken at a constant specific plastic work of 0.5 MPa subsequent to the SPC. Both definitions of the Schmitt factor match reasonably well the stress overshoot of the reloading curves. The MHH model gives the maximum stress overshoot at the correct angle, while the overall behavior is somewhat better represented by the HAH model.

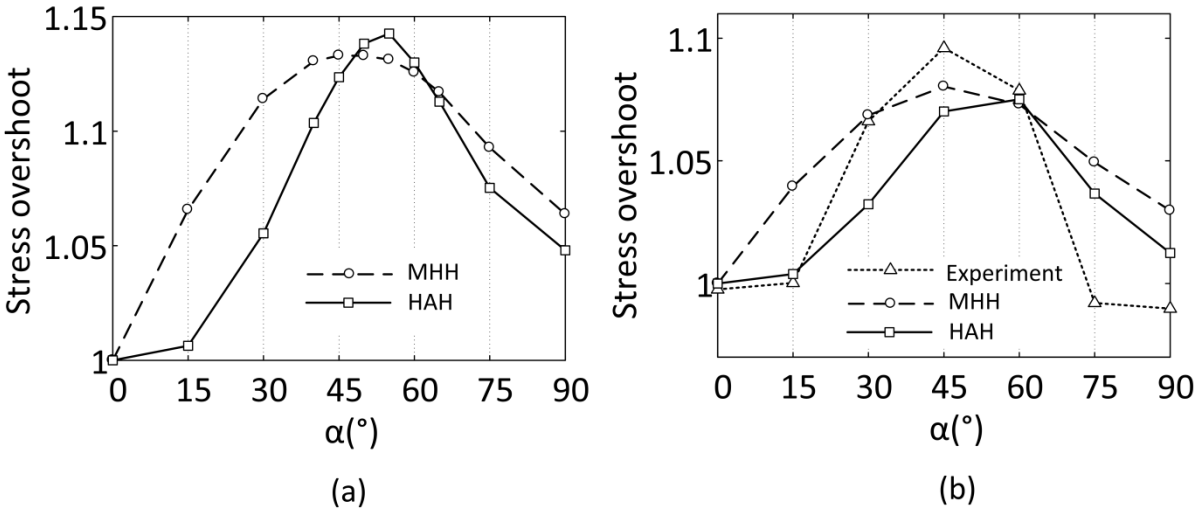


**Fig. 11**. Stress overshoot after SPC: (a) Simulated maximum stress overshoot versus direction of second strain path ($\alpha$) for EDDQ steel; (b) Stress overshoot at a specific plastic work of 0.5 MPa subsequent to SPC from simulations and experiments by Ha et al. (2013).

In **Fig. 1** and **Fig. 8**, the stress overshoot predicted by the HAH model, will be slightly lower than the experiment data. The reason is that the stress overshoot ratio controlled by $g_L$, is a little small for SPCs with Schmitt angles far from 90°. In order to compensate the reduction, orthogonal softening term is

During monotonic loading, the distorted yield surface predicted by the HAH model will expand due to work hardening, but shrink in the reverse direction relative to the loading direction. The undistorted yield surface of the MHH model will expand isotopically, but become shifted. During subsequent reverse loading, the relative shrinkage in the reverse direction will vanish and instead the yield surface of the HAH model becomes compressed in the preloading direction. Subsequent to a reverse SPC, the yield surface of the MHH model starts shifting back again and then in the opposite direction. The permanent softening subsequent to the reverse loading is obtained in a similar manner in both models, namely by reducing the isotropic work hardening during the transient response following a load reversal. The commercially pure aluminum also exhibits slight hardening stagnation after a reverse SPC. This is described by both models as an extra stress contribution during the transient behavior after load reversal. This is a new feature added to the HAH model in this work. In the MHH model, the load reversal is identified by the microstructure deviator $\mathbf{P}$ having the opposite direction of the current plastic rate-of-deformation tensor $\mathbf{D}^p$. The microstructural deviator $\bar{\mathbf{h}}$ in the HAH model does not distinguish positive and negative directions, therefore the functions $g_5$ and $g_6$ are constructed so that they contribute only during reverse transients.

During orthogonal loading, the part of the yield surface of the HAH model that is orthogonal to the first loading direction will suddenly expand and distort subsequent to the orthogonal SPC. The yield surface of the MHH model will also make a suddenly expansion, but isotropically, and in addition it will translate along the second loading direction after the orthogonal SPC. The permanent softening after an orthogonal SPC is achieved in both models by decreasing the isotropic hardening rate during the transient.

From a mathematical point of view, the need in the HAH model to make a choice of the initial direction of $\bar{\mathbf{h}}$ as the first stress direction for which plasticity occurs, is troublesome. An arbitrarily small pre-loading step, made initially in any chosen direction, would efficiently change the initial condition of $\bar{\mathbf{h}}$. This does not seem realistic. However, from a practical point

of view, the initial direction of $\bar{\mathbf{h}}$ only influences the first few percent of deformation, where Bauschinger transients anyway are very small, hence the model is applicable for most cases. The way the microstructure deviator is modeled is a major difference between the MHH and HAH models. The magnitude of $\bar{\mathbf{h}}$ in the HAH model remains constant and its rotation is restricted to a positive half-plane in the deviatoric stress space. In the MHH model, the microstructure deviator $\mathbf{P}$ is in the strain-rate space and not only its rotation, but also its magnitude evolves and is part of the modeling. The initial condition is trivial with all components equal to zero, and it may evolve in any direction, reflecting the direction and magnitude of the loading history. The two models are phenomenological, but one can interpret the microstructure deviator as a representation of the microstructure anisotropy.

The reverse tests in tension after prestraining in compression for commercially pure aluminum cf. **Fig. 2**, exhibit hardening stagnation after quite small prestrains. From the literature (Barlat et al., 2011; Haddadi et al., 2006), hardening stagnation is common and more pronounced in reverse simple shear tests after large prestrains. The modification of the HAH model offered here will predict augmented hardening stagnation with increasing prestrain as observed experimentally. But, as the HAH model was only calibrated for small prestrains in this study, more experiments are required to evaluate whether the proposed modification is applicable for large prestrains.

In the HAH model, the initial yield surface can be divided into two half-planes during preloading: an "isotropic expansion" half-plane and a "distortional shrinkage" half-plane. When reloading in the purely orthogonal direction, the R-value starts from the value prescribed by the initial yield surface (unity in this case) as the reloading direction is located in the "isotropic expansion" half-plane, as shown in **Fig. 3**. Then, the R-value evolves due to the transient, anisotropic expansion of the HAH yield surface in the orthogonal directions. When the microstructure deviator has rotated to the current strain path, the R-value again approaches unity. In the MHH model, the back stress leads to deformation-induced anisotropy even though the Hershey yield function is employed. With the evolution of the back stress, the yield surface translates in the stress space, giving an R-value different from unity after an orthogonal SPC. With further plastic straining along the new strain path, the R-value again approaches unity due to the evolution of the back stress.

The pre-distortional orthogonal softening term changes the shape of the yield surface and hence modifies the reloading R-value subsequent to SPCs. Even though this term was designed to deal with materials exhibiting orthogonal softening behavior, one might in principle gain a higher instant reloading R-value, as observed in the commercially aluminium experiments, if this term is included simultaneously as the orthogonal hardening term. Hence such a re-calibration of the orthogonal SPC of the commercially pure aluminum was tried. The orthogonal hardening parameter $L$ was adjusted to compensate for an orthogonal pre-softening by 10% ($S = 0.9$). In order to apply the pre softening term for cross hardening cases, it must vanish during a very small strain scale, of similar length as the measured R-value transient, by a very rapid initial work hardening of the re-loading curve. This requires a very large $k_S = 200$. The other model parameters are not affected and were not changed. However, it turned out that the resulting change of the initial R-value was so small for the considered yield surface, that it could hardly be distinguished from the results with only the orthogonal hardening term in **Fig. 3**. Furthermore, a negative consequence of this recalibration was that the reloading in 0° gave an even lower stress than before.

In this paper, both models have quite successfully been capable of modeling experiments for commercially pure aluminum and EDDQ steel, including various angles of single SPCs. More complex double SPCs experiments would possibly distinguish the prediction accuracy of the two models. Unfortunately such experiments have not been done along with other tests required to identify model parameters related to the yield surface, the monotonic stress-strain curve, and single and double SPCs. However, double SPCs experiments have earlier been reported for low carbon steel (Vincze et al., 2013). These results are qualitatively similar to the predictions by the HAH model for the EDDQ steel, while the MHH model behaves differently because it is restricted to isotropic expansion of the yield surface. Additional experiments are required to investigate whether a distorted yield surface can quantitatively reproduce double SPCs.

## 5. Conclusions

Two phenomenological plasticity models with potential for industrial applications to complex forming operations are evaluated with respect to describing the behavior of commercially pure aluminum and EDDQ steel during SPCs. Both models are reasonably cost effective and can qualitatively capture the transient behavior after single SPCs, i.e., the

Bauschinger effect, hardening stagnation and permanent softening after reverse SPCs, and stress overshooting and permanent softening after orthogonal SPCs. The suggested modifications of the HAH model enable simulations of the hardening stagnation after reverse SPCs and the permanent softening after orthogonal SPCs. For EDDQ steel, the MHH model gives somewhat better agreement with the available experimental data for single SPC than the HAH model for the largest prestrain. Qualitatively the HAH model can better reproduce features of double SPCs reported earlier for a low carbon steel, but more experiments are required to make a firm conclusion. For commercially pure aluminum, both models describe the single SPC with similar accuracy, but the HAH model fails to predict the transient change of the R-value subsequent to an orthogonal SPC, even if both distortional pre-softening and post expansion terms are allowed to act simultaneously.

**Funding:**

This research did not receive any specific grant from funding agencies in the public, commercial, or not-for-profit sectors.

**References**

Armstrong, P.J., Frederick, C.O., 1966. A mathematical representation of the multiaxial Bauschinger effect. Central Electricity Generating Board [and] Berkeley Nuclear Laboratories, Research & Development Department.

Barlat, F., Brem, J.C., Yoon, J.W., Chung, K., Dick, R.E., Lege, D.J., Pourboghrat, F., Choi, S.H., Chu, E., 2003. Plane stress yield function for aluminum alloy sheets - Part 1: Theory. Int. J. Plast. 19, 1297–1319.

Barlat, F., Gracio, J.J., Lee, M.-G., Rauch, E.F., Vincze, G., 2011. An alternative to kinematic hardening in classical plasticity. Int. J. Plast. 27, 1309–1327.

Barlat, F., Ha, J., Grácio, J.J., Lee, M.-G., Rauch, E.F., Vincze, G., 2013. Extension of homogeneous anisotropic hardening model to cross-loading with latent effects. Int. J. Plast. 46, 130–142.

Barlat, F., Vincze, G., Grácio, J.J., Lee, M.-G., Rauch, E.F., Tomé, C.N., 2014. Enhancements of homogenous anisotropic hardening model and application to mild and dual-phase steels. Int. J. Plast. 58, 201–218.

Bauschinger, J., 1881. Changes of the elastic limit and the modulus of elasticity on various metals. Zivilingenieur 27, 289–348.

Boers, S.H.A., Schreurs, P.J.G., Geers, M.G.D., Levkovitch, V., Wang, J., Svendsen, B., 2010. Experimental characterization and model identification of directional hardening effects in metals for complex strain path changes. Int. J. Solids Struct. 47, 1361–1374.

Boger, R.K., Wagoner, R.H., Barlat, F., Lee, M.G., Chung, K., 2005. Continuous, large strain, tension/compression testing of sheet material. Int. J. Plast. 21, 2319–2343.

Ha, J., Lee, M.-G., Barlat, F., 2013. Strain hardening response and modeling of EDDQ and DP780 steel sheet under non-linear strain path. Mech. Mater. 64, 11–26.

Haddadi, H., Bouvier, S., Banu, M., Maier, C., Teodosiu, C., 2006. Towards an accurate description of the anisotropic behaviour of sheet metals under large plastic deformations: modelling, numerical analysis and identification. Int. J. Plast. 22, 2226–2271.

Hasegawa, T., Yakou, T., Karashima, S., 1975. Deformation behaviour and dislocation structures upon stress reversal in polycrystalline aluminium. Mater. Sci. Eng. 20, 267–276.

He, J., Zeng, D., Zhu, X., Xia, Z.C., Li, S., 2014. Effect of nonlinear strain paths on forming limits under isotropic and anisotropic hardening. Int. J. Solids Struct. 51, 402–415.

Hershey, A. V, 1954. The plasticity of an isotropic aggregate of anisotropic face-centered cubic crystals. J. Appl. Mech. Asme 21, 241–249.

Holmedal, B., Berstad, T.H.O.S., 2010. Modeling transients related to strain-path changes, in: S. Kumai, O. Umezawa, Y. Takayama, T. Tsuchida, T. Sato (Eds.), 11th. International Conference of Aluminium Alloys, The Japan Institute of Light Metals. Yokohama, Japan.

Holmedal, B., Van Houtte, P., An, Y., 2008. A crystal plasticity model for strain-path changes in metals. Int. J. Plast. 24, 1360–1379.

Lee, J.-W., Lee, M.-G., Barlat, F., 2012. Finite element modeling using homogeneous anisotropic hardening and application to spring-back prediction. Int. J. Plast. 29, 13–41.

Lee, J., Kim, D., Lee, Y.-S., Bong, H.J., Barlat, F., Lee, M.-G., 2015. Stress update algorithm for enhanced homogeneous anisotropic hardening model. Comput. Methods Appl. Mech. Eng. 286, 63–86.

Levkovitch, V., Svendsen, B., 2007. Accurate hardening modeling as basis for the realistic simulation of sheet forming processes with complex strain-path changes, in: 10th ESAFORM Conference on Material Forming. AIP Publishing, pp. 358–363.

Li, F., Bate, P.S., 1991. Strain path change effects in cube textured aluminium sheet. Acta Metall. Mater. 39, 2639–2650.

Mánik, T., Holmedal, B., Hopperstad, O.S., 2015. Strain-path change induced transients in flow stress, work hardening and r-values in aluminum. Int. J. Plast. 69, 1–20.

Manopulo, N., Barlat, F., Hora, P., 2015. Isotropic to distortional hardening transition in metal plasticity. Int. J. Solids Struct. 56, 11–19.

Peeters, B., Kalidindi, S.R., Van Houtte, P., Aernoudt, E., 2000. A crystal plasticity based work-hardening/softening model for bcc metals under changing strain paths. Acta Mater. 48, 2123–2133.

Rauch, E.F., Gracio, J.J., Barlat, F., 2007. Work-hardening model for polycrystalline metals under strain reversal at large strains. Acta Mater. 55, 2939–2948.

Schmitt, J.H., Shen, E.L., Raphanel, J.L., 1994. A parameter for measuring the magnitude of a change of strain path: Validation and comparison with experiments on low carbon steel. Int. J. Plast. 10, 535–551.

Tarigopula, V., Hopperstad, O.S., Langseth, M., Clausen, A.H., 2008. Elastic-plastic behaviour of dual-phase, high-strength steel under strain-path changes. Eur. J. Mech. 27, 764–782.

Teodosiu, C., Hu, Z., 1995. Evolution of the intragranular microstructure at moderate and large strains: modelling and computational significance, in: Proc. Numiform. pp. 173–182.

Vieira, M.F., Fernandes, J.V., 1995. Plastic behaviour of copper sheets subjected to a double strain-path change. J. Mater. Process. Technol. 47, 261–272.

Vincze, G., Barlat, F., Rauch, E.F., Tomé, C.N., Butuc, M.C., Grácio, J.J., 2013. Experiments and modeling of low carbon steel sheet subjected to double strain path changes. Metall. Mater. Trans. A 44, 4475–4479.

Voce, E., 1948. The relationship between stress and strain for homogeneous deformation. J Inst Met 74, 537–562.

Yoshida, F., Uemori, T., Fujiwara, K., 2002. Elastic–plastic behavior of steel sheets under in-plane cyclic tension–compression at large strain. Int. J. Plast. 18, 633–659.

**Figure Captions:**

**Fig. 1.** Experimental and simulated stress-strain curves for commercially pure aluminum (CP-Al) from tensile tests in different directions subsequent to prestraining by rolling and tensile tests of the as-cast material.

**Fig. 2.** Experimental and simulated stress-strain curves for commercially pure aluminum (CP-Al) from tensile tests after prestraining by uniaxial compression (UC) to (a) 2% and (b) 4.4% together with the stress-strain curve for monotonic loading.

**Fig. 3.** Experimental and simulated evolution of the R-value with straining for commercially pure aluminum based on a tensile test in the transverse direction after a prestrain of 5% by rolling.

**Fig. 4.** Evolution of the yield surface of the MHH and HAH models for commercially pure aluminum: (a) uniaxial tension in the rolling direction (*x-direction*) and (b) uniaxial tension in the transverse direction (*y-direction*) subsequent to 5 % prestraining by rolling in the *x-direction*. The yield surfaces are plotted for equivalent plastic strains equal to 5 %, 10 % and 19.5 %.

**Fig. 5.** Magnitude and direction of the microstructure deviator tensors **P** and $\bar{\mathbf{h}}$ used in the MHH and HAH models, respectively, during 5% prestraining by rolling in the *x-direction* followed by uniaxial tension in the *y-direction*. The initial parallel tensors are shifted to make it possible to distinguish them in the figure.

**Fig. 6.** Experimental and simulated stress-strain curves for EDDQ steel in uniaxial tension in the 60° direction after 10 % prestraining by uniaxial tension along RD, using the original and new parameter sets for the HAH model.

**Fig. 7.** Monotonic stress-strain curve in uniaxial tension along RD for EDDQ steel.

**Fig. 8.** Stress-strain curves in uniaxial tension at various direction with respect to RD after 4 % prestraining in uniaxial tension along RD for EDDQ steel.

**Fig. 9.** Stress-strain curves in uniaxial tension at various direction with respect to RD after about 10 % prestraining in uniaxial tension along RD for EDDQ steel.

**Fig. 10.** Simulated double SPCs for EDDQ steel. The sub-figures present simulated stress-strain curves in monotonic, uniaxial tension along RD and in uniaxial tension along the 45° direction with tensile prestraining along RD. These two curves are obtained with the HAH model. The simulated stress-strain curves in uniaxial tension along RD after prestraining in tension first along RD and then along the 45° direction, are obtained by both models. The straining of the second step along the 45° direction increases from (a) to (c).

**Fig. 11.** Stress overshoot after SPC: (a) Simulated maximum stress overshoot versus direction of second strain path ($\alpha$) for EDDQ steel; (b) Stress overshoot at a specific plastic work of 0.5 MPa subsequent to SPC from simulations and experiments by Ha et al. (2013).

**Table Captions:**

**Table 1**. Model parameters for commercially pure aluminum

**Table 2** Model parameters for EDDQ steel

**Vitae:**

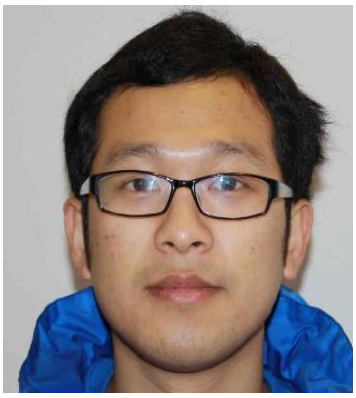

Jisheng Qin is a PhD candidate of Department of Materials Science and Engineering, Norwegian University of Science and Technology. He obtained his master's degree in 2013 from Shanghai Jiaotong University, China. Currently, he is working on modeling the plastic anisotropy induced by complex strain-path changes of aluminum and steel.

Bjørn Holmedal is a professor at Department of Materials Science and Engineering, Norwegian University of Science and Technology (NTNU). He is the leader of the physical metallurgy group at DMSE and a member of the board in the Norwegian Association of Researchers, NTNU. His works focus on Crystal plasticity (CPFEM, Taylor type models), continuum mechanics and Transients related to strain-path changes.

Dr. Kai Zhang is now a postdoc at the Norwegian University of Science and Technology, NTNU, Norway. He works on the studying, modelling and controlling extrusion microstructure of aluminum alloys. He obtained his PhD degree in 2014 from NTNU. The topic is about modelling the plastic anisotropy of aluminum alloys using advanced yield functions and crystal plasticity models.

Odd Sture Hopperstad is a professor at Department of Structural Engineering, Norwegian University of Science and Engineering (NTNU) in Trondheim, Norway. He was appointed professor at NTNU in 1998. He is a member of the Norwegian Academy of Technological Sciences and the Royal Norwegian Society of Sciences and Letters. Currently he is the Research Director of the Centre of Research-based Innovation CASA and principal investigator of the Toppforsk project FractAl at NTNU. From 2008-2011, Hopperstad was Associate Editor in International Journal of Impact Engineering. From fall 2010, he is Associate Editor in European Journal of Mechanics – A/Solids.